Submicron silicon waveguide optical switch driven by microelectromechanical actuator

doi: 10.1063/1.2892677

Submicron silicon waveguide optical switch driven by microelectromechanical actuator

Erdal Bulgan,[a] Yoshiaki Kanamori, and Kazuhiro Hane
Department of Nanomechanics, Tohoku University, 6-6-01 Aoba, Aramaki, Aoba-ku, Sendai 980-8579, Japan

(Received 2 October 2007; accepted 14 February 2008; published online 11 March 2008)

A submicron silicon waveguide optical switch driven by a microelectromechanical actuator is fabricated. The switch is composed of single-mode silicon input and output waveguides and a movable waveguide suspended by silicon springs. Switching occurs when the air gap between input and output waveguides is closed by displacing the movable waveguide 540 ± 20 nm by an electrostatic comb actuator. The switch, fabricated on a silicon-on-insulator wafer, is monolithic, and active switching region is as small as about 40×60 μm^2. An extinction ratio of 15 ± 2 dB is experimentally obtained between switch off and on states at 1.55 μm wavelength. © *2008 American Institute of Physics*. [DOI: 10.1063/1.2892677]

Because of high refractive index of silicon, confining light in a very small region is possible.[1] Sakai *et al.*,[2] for instance, have demonstrated that light at telecommunication wavelengths can propagate in a submicron silicon waveguide as small as 0.5 μm bend radius with a bend loss less than 1 dB, which suggests the potential for high-density monolithic lightwave circuits. Furthermore, an arrayed waveguide grating utilizing submicron silicon wire waveguides is fabricated into an area of 70×60 μm^2 on a silicon-on-insulator (SOI) wafer.[3] Not only realizing compact device sizes but also the ability to realize monolithic silicon-based microelectronic and optical devices on a single wafer is a very promising feature. Currently, several techniques are proposed for optical switching in submicron silicon waveguides for lightwave communication networks.[4] Mach–Zehnder interferometer type waveguide switches depending on the refractive index change induced by exerted thermal energy are reported.[5,6] Electro-optical effect of silicon is also studied for faster switching.[7,8]

Microelectromechanical systems (MEMS) are also promising for micro-optical switches. Liu *et al.*[9] have studied a planar 2×2 optical add-drop multiplexer deploying relative motion of silicon waveguides. However, the waveguides are 3 μm wide and 5 μm thick in size. Being more sophisticated, a tunable silicon microtoroidal resonator using suspended submicron silicon waveguides is also presented as coupler,[10] in which 0.69-μm-wide and 0.25-μm-thick silicon waveguides are actuated by electrostatic force. The device is wavelength dependent and is designed as an add/drop switch for wavelength division multiplexing systems. Lately, optical switches utilizing photonic crystal (PC) line-defect waveguides and microactuators are also reported.[11,12] Both devices use submicron silicon PC waveguides. The extinction ratios observed are relatively small, 10 and 4 dB, respectively, with the slow switching times of 1 ms and longer.

In this letter, we report an optical switch combining submicron silicon waveguides with a microelectromechanical actuator. The device utilizes a simple switching mechanism of physical contact[13] of waveguide tips in order to enable wavelength independent property and high extinction ratio. The proposed device is aiming future telecommunication networks as discussed in Refs. 4–6. Due to use of submicron silicon waveguides, proposed device is compact. Moreover, low mass of the movable waveguide makes switching time shorter than those of the thermo-optic switches and conventional size MEMS switches.

The proposed switch is composed of a submicron silicon input and an identical output waveguide and a movable waveguide driven by an electrostatic comb actuator, as shown schematically in Fig. 1(a). The switch is open when a voltage is not applied, as the movable waveguide is offset by the air gap from the input and output waveguides. When a voltage is applied to the actuator, movable waveguide closes the air gap. Physical contact of waveguide tips enables light propagation from the input to the output waveguide through the movable waveguide. In order to support the suspended

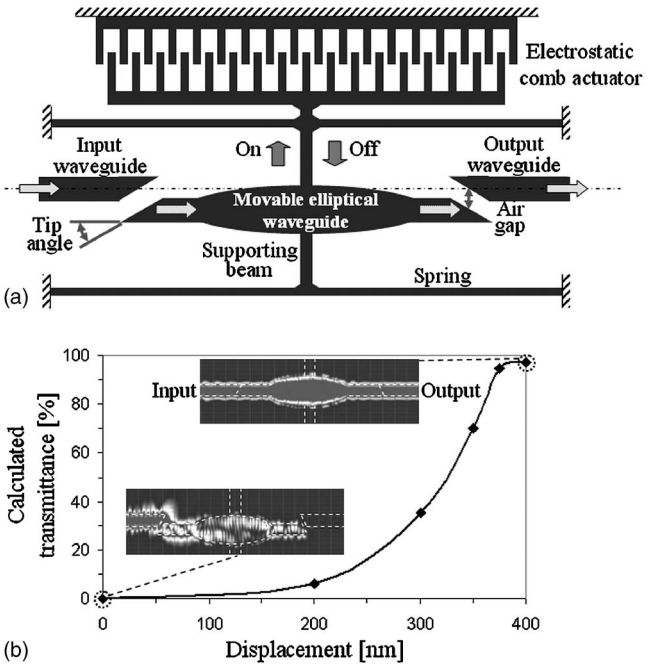

FIG. 1. (a) Schematic diagram of the optical switch. (b) Calculated transmittance as a function of displacement. The insets show the electric field intensity distribution around the movable waveguide at 0 and 400 nm displacement.

[a]Electronic mail: bulgan@hane.mech.tohoku.ac.jp.

movable waveguide in air with minimum optical transmission leak toward the supporting beams, a low-loss elliptical intersection structure[14] is deployed. The input, output, and movable waveguides are 500 nm wide and 260 nm thick, and 12.79 μm long, respectively. A doubly-clamped flexure design composed of four identical springs each 200 nm wide, 260 nm thick, and 12.15 μm long is employed in order to support the movable waveguide. The equivalent spring constant is calculated to be 0.79 N/m. The actuator is electrostatic lateral comb type and is totally 23.4×2.85 μm^2 in size. Each finger of the actuator is 1.5 μm long, 200 nm wide, and 260 nm thick. The gap between each finger pair is 200 nm and the initial finger overlap is 150 nm.

Optical property of the switch is numerically studied using three-dimensional finite-difference time-domain analysis. For single-mode TE-polarized light propagation at 1.55 μm wavelength, silicon waveguides are designed as 500 nm wide and 260 nm thick. Bottom waveguide cladding has to be thicker than 1 μm in order to keep optical propagation loss less than 0.001 dB/cm.[15] Theoretical calculation is carried out to determine the tip angle of the waveguides. It is found that the smaller the waveguide tip angle, the smaller the transmission loss during switching is. This optical property is a result of the increase of the evanescent wave penetration depth when larger tip angles are deployed. The waveguide tip angle when manufacturability is concerned is determined as 45°. Exponentially decaying evanescent waves with 110.9 nm penetration depth are calculated to arise within the tip surface boundary regions. Although the electrical fields are totally internally reflected at the angled tip surface at the switch off state, frustrated total internal reflection takes place when the movable waveguide approaches to the contact tips at the switch on state.

Figure 1(b) shows the calculated optical switch transmittance as a function of the movable waveguide displacement. Initial position of the movable waveguide is 400 nm apart from the light propagation axis of input and output waveguides. With decreasing air gap between the waveguides, transmittance increases exponentially, as shown in Fig. 1(b). Only a 400 nm in-plane displacement of the movable waveguide is calculated to yield approximately 21 dB transmittance change between on and off states. The insets in Fig. 1(b) show the electric field intensity distribution around the movable waveguide at 0 and 400 nm displacement. At 400 nm displacement, on state, the lightwave is transmitted with a small leakage mostly toward the supporting beams. At 0 nm displacement, off state, 10% of the lightwave propagates into the movable waveguide by the coupling between high-index waveguides in the evanescent region through the first air gap, but it is nearly stopped by the second gap, less than 1% reaching to the output waveguide.

In addition, spacing necessary between input and output waveguides in order to limit direct free-space transmission leak from the input to the output waveguide is investigated theoretically. The calculation suggests that a minimum of 1.6 μm spacing between input and output waveguides is sufficient to limit the leak within 1%. The calculation also reveals that when the movable waveguide fully closes the initial gap, the elliptical movable waveguide with two symmetric 500-nm wide, 260-nm thick supporting beams causes 4.6% transmission loss and 1.2% back-reflection.

Initial air gap is designed as 700 nm in order to experimentally characterize switch transmittance in a larger displacement range than that suggested as minimum theoretically. Spacing between input and output waveguides is approximately 12.29 μm. Resultant active switching region is as small as about 40×60 μm^2.

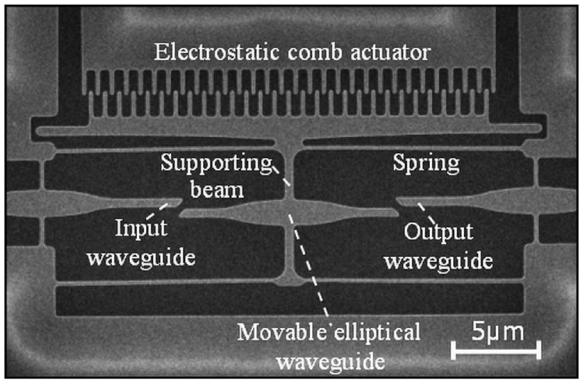

FIG. 2. Fabricated optical switch.

The switch is fabricated on a SOI wafer with 260-nm-thick device silicon and 2-μm-thick buried-oxide layers. Spring width, 200 nm, is the smallest dimension in the proposed design. First, switch geometry is patterned using electron beam lithography (EB 5000LSS, JEOL Co.). A positive electron beam resist (ZEP520A, ZEON Corp.) is spin coated. Hexamethyl disilazane (OAP, Tokyo Ohka Kogyo Co.) is utilized as an interface layer between device silicon and the resist for improving the patterning quality. Then, device silicon layer is dry etched by fast atom beam (Ebara Research Co.) using SF_6 gas. Finally, the switch is released by vapor HF etching with the advent of substrate stiction prevention.

Due to small device size, displacement of the actuator is measured as a function of applied voltage under scanning electron microscope (SEM). In optical testing of the switch, a tunable laser (HP Agilent 81682A) is used as the light source. TE-like polarized light at 1.55 μm wavelength is coupled into the input waveguide by an objective lens. The switch is observed from the top with an infrared (IR) camera (C2741, Hamamatsu Photonics). Switch output is evaluated from the spot intensity of scattered light observed at 45°-cut edge of the output waveguide by a custom software instead of measuring at the end of the silicon output waveguide.

Fabricated switch is shown in Fig. 2. The springs and movable elliptical waveguide are properly fabricated. Nevertheless, owing to residual stress release of single crystalline silicon, springs are observed to shift about 160 ± 20 nm in-plane toward the actuator in the SEM chamber. Dynamic characterization of the actuator reveals a fundamental resonance frequency of 109 kHz.

Figures 3(a) and 3(b) show the IR camera images of the active switching region at off and on states, respectively. Schematic diagram of the switch and SEM images of the waveguide ends during actuation are also shown as insets in Fig. 3. The leftmost light spots in Figs. 3(a) and 3(b) are switch output signals at off and on states, respectively. The output is observed to increase when the switch is turned on by closing the air gap with the movable waveguide. Extinction ratio of transmittance is experimentally found to be 15 ± 2 dB between off and on states. While going from the input toward the output in Fig. 3, first light spot is the scattered light at the input/movable waveguide contact (SL_1), second light spot is the scattered light at the movable/output

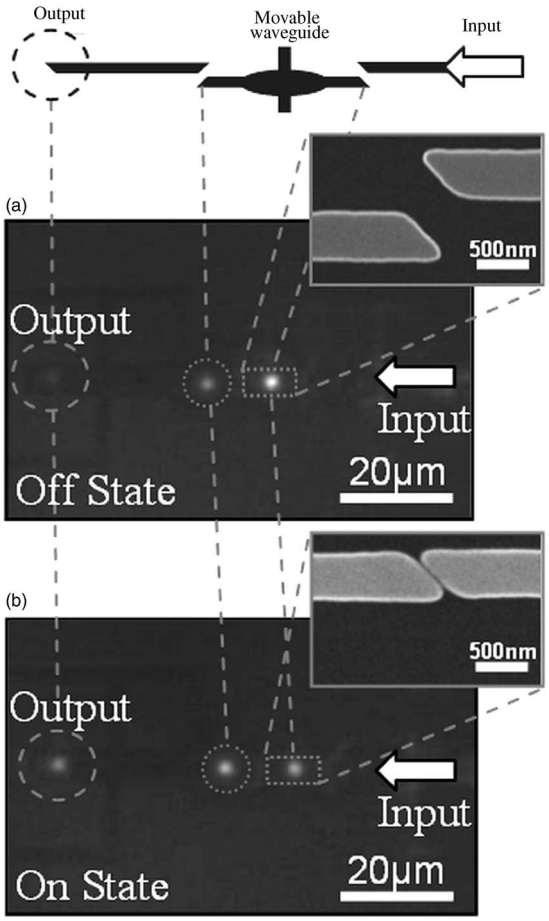

FIG. 3. Infrared camera images of the switch. (a) Off state at 0 V. (b) On state at 65 V, corresponding to approximately 540 nm movable waveguide displacement.

waveguide contact pair (SL_2). At the off state, SL_1 is greater than SL_2 due to the transmission losses caused by the air gaps. Once the switch is turned on, SL_1 and SL_2 decrease to zero in theory because of increasing transmittance from the input to the movable waveguide due to smaller air gap. However, due to patterning imperfections at the angled tips of waveguides and a small tilt of the movable waveguide during actuation, they do not become zero. Further improvement of the contact surfaces and movable waveguide alignment will reduce losses at the contact.

Measured switch transmittance as a function of both movable waveguide displacement and actuation voltage is plotted in Fig. 4. The transmittance increases gradually with the movable waveguide displacement up to approximately 540 nm. The relative dependence of the measured output on the displacement shown in Fig. 4 is explained by the calculated transmittance shown in Fig. 1(b). Around 400 nm of displacement, the transmittance fluctuates slightly owing to an in-plane tilting of the movable waveguide. Measured devices yield 27.4% switch transmittance, meaning 52.3% transmittance at each contact pair, at 540 nm displacement at 65 V voltage.

In order to investigate the achievable extinction ratio, we fabricated switch structures without the actuator. Fabricated structures have fixed-air gaps of 0, 100, 200, and 400 nm. From the measured outputs, an extinction ratio of approximately 21.6 dB is estimated at 540 nm displacement. Further increase in extinction ratio is feasible by increase in actuator's displacement in the proposed switch.

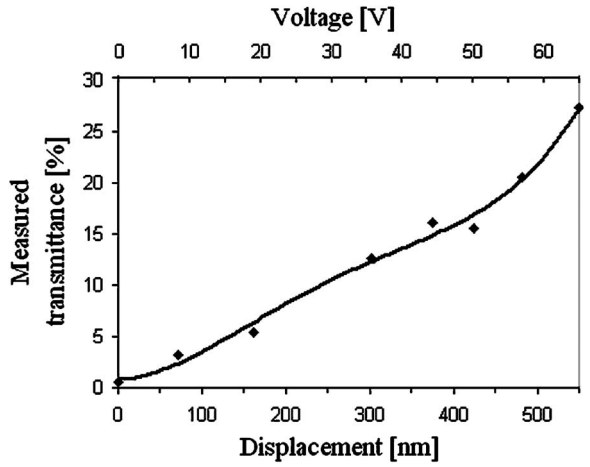

FIG. 4. Measured transmittance as a function of both actuation voltage and displacement.

In conclusion, a submicron single-mode silicon waveguide microelectromechanical optical switch is designed, fabricated, and tested. The switch utilizes physical contact of silicon waveguide tip pairs. Active switching area is as small as about $40 \times 60\ \mu m^2$. Approximately 27% on-state optical transmittance is obtained at 65 V actuation voltage corresponding to 540 nm displacement. An extinction ratio of 15 ± 2 dB is experimentally observed between off and on states. The resonance frequency of the movable waveguide is 109 kHz, which can generate much faster switch response than conventional MEMS switches. The proposed switch is expected to be useful in the lightwave communication networks.

[1] B. Jalali and S. Fathpour, J. Lightwave Technol. **24**, 4600 (2006).
[2] A. Sakai, G. Hara, and T. Baba, Jpn. J. Appl. Phys., Part 2 **40**, L383 (2001).
[3] K. Sasaki, F. Ohno, A. Motegi, and T. Baba, Electron. Lett. **41**, 801 (2005).
[4] M. C. Wu, O. Solgaard, and J. E. Ford, J. Lightwave Technol. **24**, 4433 (2006).
[5] R. L. Espinola, M.-C. Tsai, J. T. Yardley, and R. M. Osgood, IEEE Photonics Technol. Lett. **15**, 1366 (2003).
[6] T. Chu, H. Yamada, S. Ishida, and Y. Arakawa, Opt. Express **13**, 10109 (2005).
[7] L. Liao, D. Samara-Rubio, M. Morse, A. Liu, D. Hodge, D. Rubin, U. D. Keil, and T. Franck, Opt. Express **13**, 3129 (2005).
[8] M. Lipson, IEEE J. Sel. Top. Quantum Electron. **12**, 1520 (2006).
[9] X. Liu, J. Kubby, J. Chen, J. Diehl, K. Feinberg, K. German, P. Gulvin, L. Herko, N. Jia, P. Lin, J. Ma, J. Meyers, P. Nystrom, and Y. R. Wang, J. Vac. Sci. Technol. A **22**, 826 (2004).
[10] J. Yao, D. Leuenberger, M. M. Lee, and M. C. Wu, IEEE J. Sel. Top. Quantum Electron. **13**, 202 (2007).
[11] S. Iwamoto, S. Ishida, Y. Arakawa, M. Tokushima, A. Gomyo, H. Yamada, A. Higo, H. Toshiyoshi, and H. Fujita, Appl. Phys. Lett. **88**, 011104 (2006).
[12] K. Umemori, Y. Kanamori, and K. Hane, Appl. Phys. Lett. **89**, 021102 (2006).
[13] M. Kihara, S. Nagasawa, and T. Tanifuji, J. Lightwave Technol. **14**, 542 (1996).
[14] T. Fukazawa, T. Hirano, F. Ohno, and T. Baba, Jpn. J. Appl. Phys., Part 1 **43**, 646 (2004).
[15] G. T. Reed and A. P. Knights, *Silicon Photonics: An Introduction* (Wiley, New York, 2004), p. 76.